

# Supporting Information

Lavigne et al. 10.1073/pnas.1307520110

## SI Materials and Methods

**Radiocarbon Dating.** Samples of charcoal were prepared at the  $^{14}\text{C}$  laboratory, Eidgenössische Technische Hochschule Zurich, before accelerator mass spectrometry (AMS) analyses. Contamination by extraneous carbon was removed using the standard Acid Alkali Acid treatment (1). Charcoal was immersed in a weak acid bath (0.5 M HCl) at 60 °C for 12 h, removing carbonates. Following multiple washes in distilled water, the samples were treated with a weak base (0.1 M NaOH) at 60 °C for 12 h. This process removes humic acids that might also contaminate the sample. The samples were next washed at neutral pH. A final acid wash was applied to remove any atmospheric carbon that might have bonded to the charcoal during base treatment. The dried samples (1 mg of C) were converted to graphite, pressed into the targets and analyzed using AMS along with a set of blank and standards. Blanks made of  $^{14}\text{C}$ -free coal were prepared to monitor contamination during the preparation process. Conventional  $^{14}\text{C}$  ages (Fig. 4) were calculated following Stuiver and Polach (2). These ages include correction for fractionation based on on-line measurements of  $\delta^{13}\text{C}$  on graphite. The 1- $\sigma$  error includes counting uncertainty as well as the scatter of standards and blanks.  $^{14}\text{C}$  ages were calibrated using the OxCal 4.1 program and INTCAL09 calibration dataset. We also applied the Bayesian model of OxCal 4.1 that puts constraints on the ages (prior) (3) to obtain a more precise chronology.

**Modeling the Caldera Size.** We modeled the size of the Samalas eruption based on pre- and posteruption topography of the Rinjani Volcanic Complex (hereafter RVC). This process of course required reconstruction of the preeruptive topography as follows (4):

- i) We located cells in the digital elevation model (DEM) likely to represent the pre-eruptive surface. They include plateaus, sectors of volcano preserved from erosion, and crests that are the uppermost interfluvies remaining after a significant amount of erosion. These sites provide the best approximation of paleotopography.
- ii) The preeruption RVC topography is first modeled from these located points by defining a first-order radial surface. It is a kind of surface of revolution defined by: (i) an exponential-like function (the generatrix) fitting the average concave-upwards volcano profile; and (ii) the volcano's summit location, around which the generatrix is rotated to form the surface. To obtain the best-fitting first-order surface, we introduce the following sophistication. A conventional surface of revolution with axial symmetry generates circular contour lines. Instead, as the generatrix rotates around the summit location, we stretch and contract it to obtain, in planar section, an elliptically shaped surface defined by elliptical contour lines. The optimal set of parameters that define the first-order primary volcanic surface is obtained by a least-squares method using the simplex algorithm (5). Parameters solved for include the location and elevation of the volcano summit, the eccentricity and long-axis azimuth of the contour lines, and the coefficients of the generatrix.
- iii) The first-order geometric surface is then modified according to second-order elevation variations because of local distributions of volcanic products. Residuals between elevations of the input points selected as representative of the preeruption surface and those obtained by the first-order modeled surface are calculated. Residuals are interpolated by kriging and next summed to the first-order surface elevations to obtain the

definitive preeruption surface elevation. Two independent surfaces are modeled for each of the two RVC volcanoes. The preeruption surface elevation of RVC is finally obtained by retaining for each of the two volcanoes, the area and elevations where the modeled paleo preexplosion surface lies above the postexplosion lower surface. Kriging adjustments also yield SEs for elevations of both basal and upper surfaces that provide a measure of the uncertainty in the calculated volume of material removed by the Samalas eruption.

In addition to the preeruption surface, modeled as described above, calculation of the missing volume requires knowing the elevation of the caldera base everywhere immediately after the eruption. The present caldera walls provide some constraints on this but within the crater, the floor has been mantled in products of the Samalas eruption and subsequent activity of Gunung Barujari (in the past two centuries). The basal surface is interpolated by kriging from the DEM cells located on the caldera walls but the lack of constraints on the thicknesses of accumulated material in the caldera limits its reliability.

Finally, for every DEM cell, the height difference between elevations of the preeruptive surface and caldera basal surface is multiplied by the cell area. We estimate uncertainty by similarly calculating the product of height difference SEs and cell area. The final calculation of the volume of removed material requires summation of each cell volume, and summation of errors.

**Written Sources. Translation to Indonesian and to English of the historic poem Babad Lombok, written in the Old Javanese language.** The original text of the historic poem *Babad Lombok* in Old Javanese language, Wacana (6):

274. *Gunung Rinjani kularat, miwah gunung samalas rakrat, balabur watu gumuruh, tibeng desa Pamatan, yata kanyut bale haling parubuh, kurambangning sagara, wong ngipun halong kang mati.*

275. *Pitung dina lami nira, gentuh hiku hangebeki pretiwi, hing leneng hadampar, hanerus maring batu Dendeng kang nganyuk, wong ngipun kabeh hing paliya, saweneh munggah hing ngukir.*

276. *Hing jaringo hasingidan, saminya ngungsi salon darak sangaji, hakupul hana hing riku, weneh ngungsi samuliya, boroh Bandar papunba lawan pasulun, sarowok pili lan ranggiya, sambalun pajang lan sapit.*

277. *Yek nango lan pelameran, batu banda jejangkah tanah neki, duri hanare menyan batu, saher kalawan balas, batu lawang batu rentang batu cangku, samalih tiba hing tengah, brang bantuan gennira ngungsi.*

278. *Hana ring pundung buwak bakang, tana' gadang lembak babidas hiki, saweneh hana halarut, hing bumi kembang kekrang, pangadangan lawan puka hatin lungguh, saweneh kalah kang tiba, mara hing langko pajanggih.*

279. *Warnanen kang munggend palowan, sami larut lawan ratu hing nguni, hasangidan ya riku, hing Lombok goku medah, genep pitung dina punang gentuh, nulih hangumah desa, hing preneha siji-siji.*

The Indonesian translation of the historic poem *Babad Lombok*:

274. *Gunung Rinjani Longsor, dan Gunung Samalas runtuh, banjir batu gemuruh, menghancurkan Desa Pamatan, rumah2 rubuh dan hanyut terbawa lumpur, terapung-apung di lautan, penduduknya banyak yang mati.*

275. Tujuh hari lamanya, gempa dahsyat meruyak bumi, terdampar di Leneng (lenek), diseret oleh batu gunung yang hanyut, manusia berlari semua, sebahagian lagi naik ke bukit.

276. Bersembunyi di Jeringo, semua mengungsi sisa kerabat raja, berkumpul mereka di situ, ada yang mengungsi ke Samulia, Borok, Bandar, Pepumba, dan Pasalun, Serowok, Piling, dan Rangi, Sembalun, Pajang, dan Sapit.

277. Di Nangan dan Palemoran, batu besar dan gelundungan tanah, duri, dan batu menyan, batu apung dan pasir, batu sedimen granit, dan batu cangku, jatuh di tengah daratan, mereka mengungsi ke Brang batun.

278. Ada ke Pundung, Buak, Bakang, Tana' Bea, Lembuak, Bebidas, sebagian ada mengungsi, ke bumi Kembang, Kekrang, Pengadangan dan Puka hate-hate lungguh, sebagian ada yang sampai, datang ke Langko, Pejanggik.

279. Semua mengungsi dengan ratunya, berlindung mereka di situ, di Lombok tempatnya diam, genap tujuh hari gempa itu, lalu membangun desa, di tempatnya masing-masing.

The English translation of the historic poem *Babad Lombok*:

274. Mount Rinjani avalanched and Mount Salamas collapsed, followed by large flows of debris accompanied by the noise coming from boulders. These flows destroyed (the seat of the kingdom) Pamatan. All houses were destroyed and swept away, floating on the sea, and many people died.

275. During seven days, big earthquakes shook the Earth, stranded in Leneng (Lenek), dragged by the boulder flows, People escaped and some of them climbed the hills.

276. Hiding in Jeringo (close to Mataram), all people moved with the rest of the king's family to several places: Samulia, Borok, Bandar, Pepumba Pasalun, Serowok, Piling, and Rangi, Sembalun, Pajang, and Sapit.

277. At Nangan and Palemoran, big boulders rolled with soil, with pumices and sand, and granite sediments on the land, they evacuated to Brang Batun.

278. There were people moving to Pundung, Buak, Bakang, Tana Bea, Lembuak, Bebidas, some of them evacuated to Kembang Bumi, Kekrang, Pengadangan and Puka Puka hate-hate lungguh and also to Langko and Pejanggik.

279. Everybody took refuge together with the King, Lombok became very quiet, even seven days after the earthquakes occurred, and later they built their own houses.

1. Hajdas I (2009) Applications of radiocarbon dating method. *Radiocarbon* 51(1):79–90.
2. Stuiver M, Polach HA (1977) Reporting of C-14 data—Discussions. *Radiocarbon* 19(3): 355–363.
3. Ramsey CB (2009) Analyses of radiocarbon dates. *Radiocarbon* 51(1):337–360.
4. Lahitte P, Samper A, Quidelleur X (2012) DEM-based reconstruction of Southern Basse-Terre volcanoes (Guadeloupe archipelago, FWI): Contribution to the Lesser Antilles arc construction rates and magma production. *Geomorphology* 136(1): 148–164.
5. Nelder JA, Mead RA (1965) A simple method for function minimization. *Comput J* 7: 308–313.
6. Wacana L (1979) *Babad Lombok*. (Departemen Pendidikan dan Kebudayaan, Proyek Penerbitan Buku Bacaan dan Sastra Indonesia dan Daerah, Jakarta).

## Evidence for Northern Hemisphere Winter Warming in Western Europe in 1257/1258. Arras (France).

*En cest an, fut le temps si douz et si souef (chaud) que en tout l'hiver ne gela que deux jours : ou mois de janvier, trouvoit on des violettes et les fleurs de fraisiers, et estoient tous les pommiers tous blancs flouris.* (7)

Translation: At that time the wheater was so mild and so hot that frost barely lasted for more than two days. In January [1258], violets could be observed, and strawberries and apple trees were in blossom.

## Paris (France).

*Et en l'autre année après, qui est en l'incarnation par M.CC. et LVI (1256) fist trop durement fort hyvier ou royaume de France et pluvieux esté dusqu'à la Nativité saint Jehan Baupstiste (24 juin). Et en l'autre année après, fist merveilleusement chaut esté et chaut temps jusqu'à la Chandeleur ; et puis après, fist merveilleusement grant froit jusqu'à la saint Marc (25 avril). Et en cèle année meïsmes, ot par toute la France grant chierté de pain, de vin et de toutes viandes.* (8)

Translation: And the following year, which is the year 1256 of the Incarnation, the winter was very harsh in the kingdom of France and the summer was very rainy until the Nativity of Saint Jean Baptist (June 24). And the following year (1257), the summer was excessively hot, and the weather was warm until Candlemass (2 February 1258), and then it was excessively cold until the St. Mark (25 April 1258). And this year also, there was throughout France a great shortage of bread, wine and any meat.

## Saint Alban Abbey (England).

*Annus quoque iste, cronicarum infirmitatum genitivus vix occupatum permisit aliquatenus respirare. Non enim frigus vel serenitas vel gelu saltem aliquantulum stagnorum superficiem, prout consuevit, glaciale m induravit, vel stiriam a stillicidiis coegit dependere ; sed continuae inundationes pluviarum et nebularum usque ad Purificationem beatae Virginis aera inspissarunt.* (8)

Translation: This year (1257), too, generated chronic complaints, which scarcely allowed free power of breathing to any one labouring under them. Not a single frosty or fine day occurred, nor was the surface of the lakes at all hardened by the frost, as was usual; neither did icicles hang from the ledges of houses; but uninterrupted heavy falls of rain and mist obscured the sky until the Purification of the Blessed Virgin (2 February 1258) (10)

7. Delisle L, Jourdain CMG, Wailly DEN, eds (1877) *Chronique Anonyme Finissant en 1306. Tome 21, Recueil des historiens des Gaules et de la France* (Victor Palmé, Paris), pp. 130–137.
8. Delisle L, Jourdain CMG, Wailly DEN eds (1877) *Chronique Anonyme des Rois de France Finissant en 1286. Tome 21, Recueil des historiens des Gaules et de la France*, (Victor Palmé, Paris) pp. 81–102.
9. Luard HR ed (1872–1873) *Matthaei Parisiensis monachi sancti Albani Chronica Majora Rerum britannicarum medii aevi scriptores Vol. 5* (London) pp. 661–662.
10. Giles JA ed and trans (1854) *Matthew Paris's English History. From the Year 1235 to 1273 Vol. 3* (Henry G. Bohn, London) pp. 256–257.





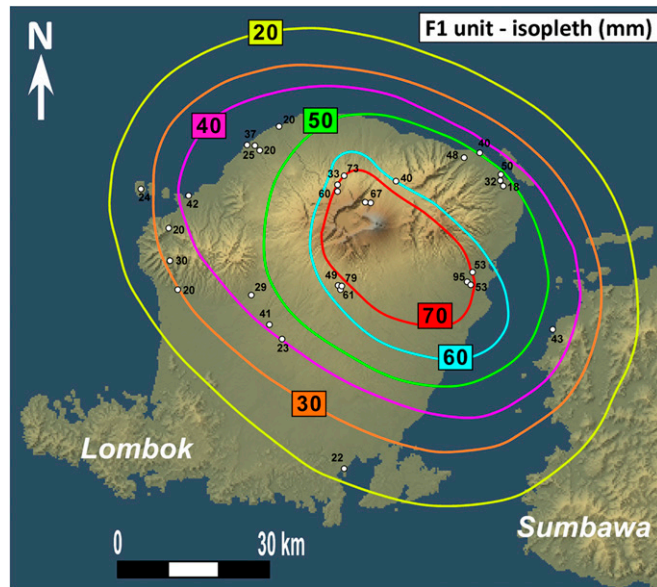


**Fig. S3.** Maximum pumice  $M_P$  isopleths (mm) for the F1 Plinian pumice fallout unit of the Samalas eruption. The presence of pumice clasts of up to 50 mm at 46-km distance SE from the vent on Sumbawa attests to the large magnitude of the F1 ultraplinian phase of the Samalas eruption. This tendency is confirmed by the limited  $M_L$  dataset that shows lithics of up to 35 mm at 27 km SE from the source on the eastern coastline of Lombok.



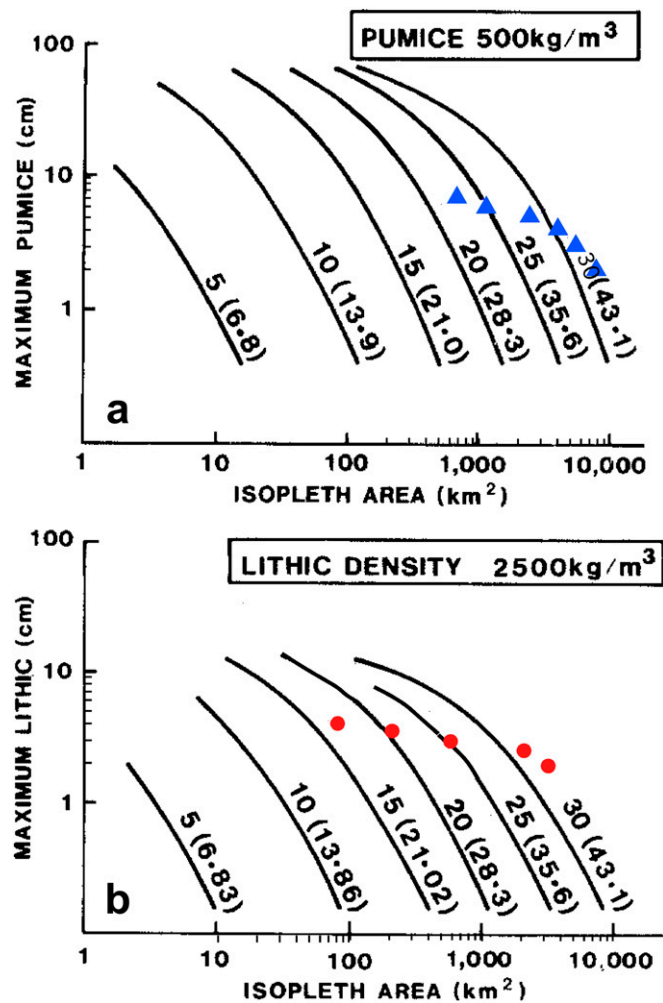


**Fig. 55.** Maximum height ( $H_t$ ) of the column for the plinian F1 phase of the mid-13<sup>th</sup> century eruption of Samalas volcano. The maximum height  $H_T$  of the column was estimated as  $\sim 43 \text{ km} \pm 8.6 \text{ km}$  using the model of Carey and Sparks (1) and the data for the 2 and 3 cm isopleths for pumice clasts (A). Limited data from the maximum lithic clast 2.4 cm isopleth (B) yield a minimum  $H_T$  value of 43 km (no lithic clasts larger than 2.4 cm were found in distal parts of the deposit). Column heights on the curves are shown in km as  $H_T$  ( $H_B$ ), for example 25 (35.6), with  $H_T$  the total column height and  $H_B$  the height of neutral buoyancy of the column. These data correspond to a neutral buoyancy  $H_B$  height of 30 km derived, respectively, from the pumice and lithic isopleths for the F1 fallout unit and based on empirical relationships from Sparks (2) and Pyle (3). The geometry of the pumice isopleths shows, according to theoretical relationships of Carey and Sparks (1), that the F1 convective column formed in a strong crosswind with estimated velocity  $> 20 \text{ m.s}^{-1}$  as determined using 0.8-cm diameter clasts with a density of  $2500 \text{ kg.m}^{-3}$ , which are equivalent to the F1 pumice clasts of 4 cm diameter and a clast density of  $500 \text{ kg.m}^{-3}$  higher but compatible with the density of the Samalas F1 pumice of  $380 \text{ kg.m}^{-3}$ .

- Carey S, Sparks RSJ (1986) Quantitative models of fallout and dispersal of tephra from volcanic eruption columns. *Bulletin of Volcanology* 48(109):109–125.
- Sparks RSJ (1986) The dimension and dynamics of volcanic eruption columns. *Bulletin of Volcanology* 48(1):3–15.
- Pyle DM (2000) Sizes of volcanic eruptions. in *Encyclopedia of Volcanoes*. (Academic Press, San Diego) pp. 263–269.

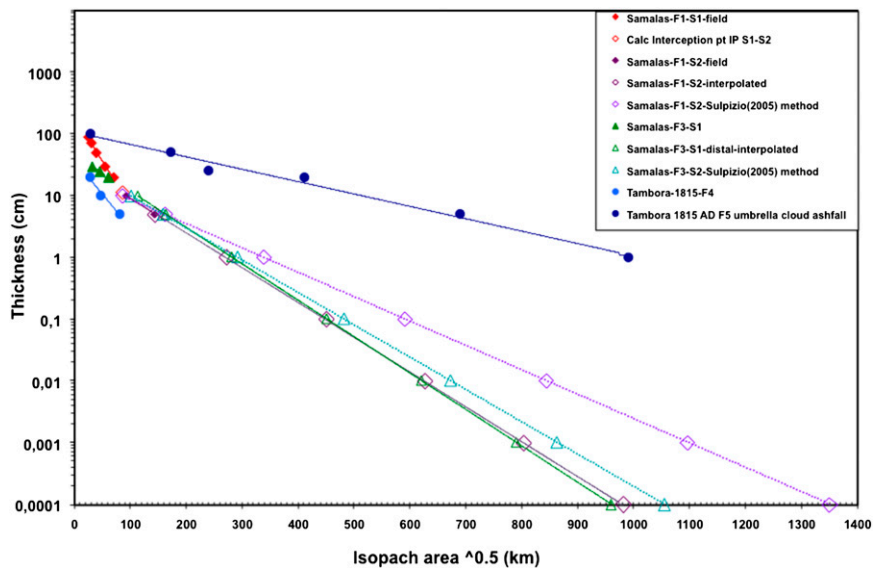


**Fig. 56.** Log isopach thickness versus isopach area<sup>0.5</sup>. The exponential thinning of pumice fallout deposits for the Samalas F1 and F3 Plinian pumice fallout units allows a determination of the total erupted volume and its uncertainty using methodologies developed by Pyle (1), Sulpizio (2), and Fierstein and Nathenson (3). The uncertainty in the distal volume of units F1 and F3 is largely controlled by the slope of the distal segment S2 (dotted lines) of the exponential thinning law (the lower the slope, the greater the distal volume) in the volume computation following the methodology of Fierstein and Nathenson (3). The volume data is compared to the Tambora F4 Plinian fallout unit and the F5 umbrella cloud ash fallout unit, modified after Sigurdsson and Carey (4) and Self et al. (5).

1. Pyle DM (2000) Sizes of volcanic eruptions. *Encyclopedia of Volcanoes*, eds Sigurdsson H, Houghton B, Rymer H, Stix J, McNutt S (Academic, San Diego), pp 263–269.
2. Sulpizio R (2005) Three empirical methods for the calculation of distal volume of tephra-fall deposits. *J Volcanol Geotherm Res* 145(3-4):315–336
3. Fierstein J, Nathanson M (1992) Another look at the calculation of fallout tephra volume. *Bull Volcanol* 54(2):156–167.
4. Sigurdsson H, Carey S (1989) Plinian and co-ignimbrite tephra fall from the 1815 eruption of Tambora volcano. *Bull Volcanol* 51(4):243–270.
5. Self S, Gertisser R, Thordarson T, Rampino MR, Wolff JA (2004) Magma volume, volatile emissions, and stratospheric aerosols from the 1815 eruption of Tambora. *Geophys Res Lett* 31: L20608.

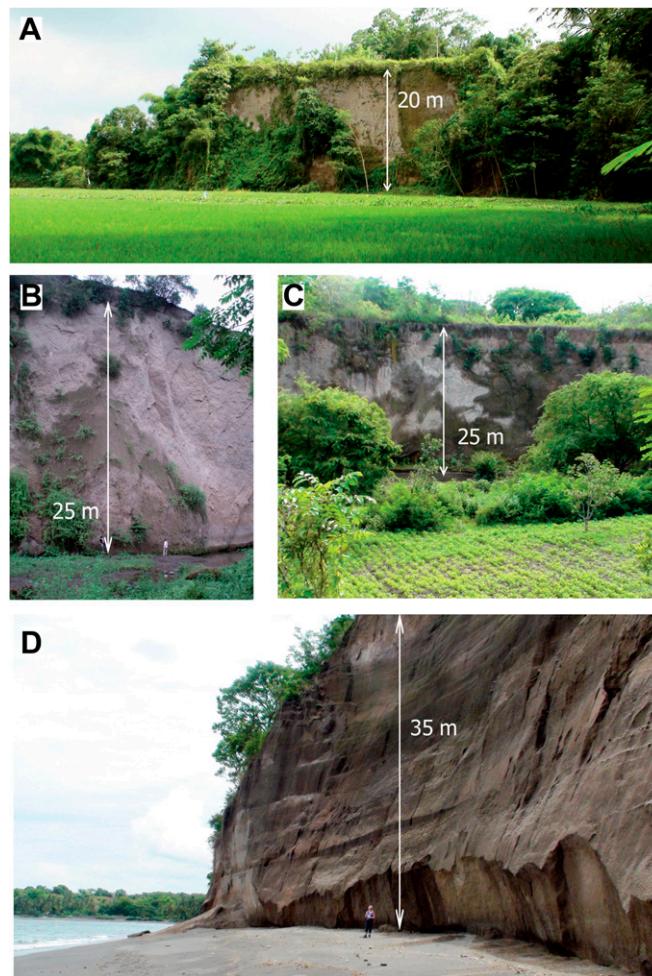


**Fig. S7.** Pyroclastic density current (PDC) deposits emplaced during the 13th eruption of Samalas. (A) Sedau village, southwest flank, 22 km from the caldera rim. (B and C) North flank, 20 km from the caldera rim. (D) Pumice cliff on the northwest coast of Lombok (photos: A, C, and D courtesy of F.L.; B courtesy of J.-P.D.). Between 10 and 20 km from the caldera rim, ignimbrites are deeply downcut by rivers (A–C). Successions of PDC and pyroclastic-fall deposits from the 13th century eruption form the entire valley walls up to thicknesses of 30 m. The Samalas PDCs entirely modified the precaldera topography, filling former valleys, and resulting in relief inversion following subsequent erosion. On the northwest coast, a remnant of the ignimbrite at 23 km from the caldera rim forms a 35-m-high recessive cliff (D), suggesting that a substantial part of the PDCs entered the sea.

**Table S1. The largest well-documented volcanic eruptions ( $M > 5$ ) during the Holocene**

| Volcano                 | Country               | Deposit name                   | Bulk deposit volume (km <sup>3</sup> ) | DRE volume (km <sup>3</sup> ) | Adjusted mass (kg)                                  | Mass eruption rate (kg/s)            | Maximum magnitude* | Intensity <sup>†</sup> | Age                  | Source                     |
|-------------------------|-----------------------|--------------------------------|--|-------------------------------|---|--------------------------------------|--------------------|------------------------|----------------------|----------------------------|
| Kurile Lake             | Kamchatka, Russia     | KO                             | 170                                    | 80                            | $1.92 \times 10^{14}$                               |                                      | 7.3                |                        | 6460–6414 cal B.C.   | (1)                        |
| Santorini               | Greece                | Minoan <sup>‡</sup>            |  | 60                            | $1.48 \times 10^{14}$                               | $2.50 \times 10^8$                   | 7.2                | 11.4                   | 1627–1600 cal B.C.   | (2, 3)                     |
| Mazama (Crater Lake)    | Oregon, United States | Lower pumice <sup>‡</sup>      |  | 52                            | $1.28 \times 10^{14}$                               |                                      | 7.1                |                        | 5677 cal B.C.        | (4, 5)                     |
| <b>Samalas</b>          | <b>Indonesia</b>      | <b>1257 A.D.<sup>‡ 5</sup></b> |  | <b>&gt;40</b>                 | <b><math>9.90 \times 10^{13}</math><sup>¶</sup></b> | <b><math>1.10 \times 10^9</math></b> | <b>7.0</b>         | <b>12.0</b>            | <b>Cal A.D. 1257</b> | <b>Present work (6, 7)</b> |
| Ilopango                | El Salvador           | Tierra Blanca Joven            | 84                                     | 39                            | $8.15 \times 10^{13}$                               |                                      | 6.9                |                        | Cal A.D. 536         |                            |
| Tambora                 | Indonesia             | A.D. 1815 <sup>‡</sup>         |  | >33                           | $8.15 \times 10^{13}$                               | $2.8 \times 10^8$                    | 6.9                | 11.4                   | A.D. 1815            | (8, 9)                     |
| Taupo                   | New Zealand           | A.D. 180                       | 105                                    | 35                            | $8.00 \times 10^{13}$                               | $1.10 \times 10^9$                   | 6.9                | 12.0                   | A.D. $232 \pm 5$     | (8, 10, 11)                |
| Aniakchak               | Alaska, United States | 3430 B.P.                      |  | 27                            | $6.21 \times 10^{13}$                               |                                      | 6.8                |                        | 1645 B.C.            | (12–14)                    |
| Changbaishan/Baitoushan | China/North Korea     | Millenium eruption             | 96                                     | 24.5                          | $5.64 \times 10^{13}$                               |                                      | 6.8                |                        | Cal A.D. 946         | (15, 16)                   |
| Quilotoa                | Ecuador               | 800 B.P.                       | 21.3                                   | 18.7                          | $4.22 \times 10^{13}$                               | $2.00 \times 10^8$                   | 6.6                | 11.3                   | Cal A.D. 1275        | (17, 18)                   |
| Katmai - Novarupta      | Alaska, United States | Valley of 10 000 Smokes        | 17                                     | 6.8                           | $3.00 \times 10^{13}$                               | $1.00 \times 10^8$                   | 6.5                | 11.0                   | A.D. 1912            | (8, 19)                    |
| Krakatau                | Indonesia             | A.D. 1883                      | 18–21                                  | 12.5                          | $3.00 \times 10^{13}$                               | $5.00 \times 10^7$                   | 6.5                | 10.7                   | A.D. 1883            | (8, 20)                    |
| Santa Maria             | Guatemala             | A.D. 1902                      | 20.2                                   | 8.6                           | $2.00 \times 10^{13}$                               | $1.70 \times 10^8$                   | 6.3                | 11.2                   | A.D. 1902            | (8, 21)                    |
| Quizapu                 | Chile                 | A.D. 1932                      | 9.5                                    | 4                             | $9.72 \times 10^{12}$                               | $1.50 \times 10^8$                   | 6.0                | 11.2                   | A.D. 1932            | (22)                       |
| Pinatubo                | Philippines           | A.D. 1991                      |  | 5                             | $1.10 \times 10^{13}$                               | $4.00 \times 10^8$                   | 6.0                | 11.6                   | A.D. 1991            | (8)                        |
| Vesuvius                | Italy                 | A.D. 79                        |  | 3.25                          | $6.00 \times 10^{12}$                               | $1.50 \times 10^8$                   | 5.8                | 11.2                   | A.D. 79              | (8, 23)                    |
| Rungwe                  | Tanzania              | Rungwe pumice                  | 3.2–5.8                                | 1.4                           | $2.00 \times 10^{12}$                               | $4.80 \times 10^8$                   | 5.3                | 11.7                   | ca. 4000 B.P.        | (24)                       |
| Huaynaputina            | Peru                  | A.D. 1600 Stage I              | 7                                      | 2.6                           | $1.30 \times 10^{12}$                               | $2.40 \times 10^8$                   | 5.1                | 1.4                    | A.D. 1600            | (25)                       |
| Chichon                 | Mexico                | Unit B 550 BP                  | 2.8                                    | 1.1                           | $1.05 \times 10^{12}$                               | $1.00 \times 10^8$                   | 5.0                | 11.0                   | Cal A.D. 1320–1433   | (26)                       |

\* $M = \log_{10}(\text{erupted mass kg}) - 7$ .

<sup>†</sup> $I = \log_{10}(\text{mass eruption rate kg/s}) + 3$ .

<sup>‡</sup>Erupted mass is taken assuming an average of 2,470 kg-m<sup>3</sup> for the dense-rock equivalent (DRE) density like for Samalas and Tambora.

<sup>5</sup>Minimum magnitude as uncertainty on distal to very distal ash bulk volume is significant.

<sup>¶</sup>Minimum value, that of the calculated missing caldera.

- Ponomareva VV, et al. (2004) The 7600 (14C) year BP Kurile Lake caldera-forming eruption, Kamchatka, Russia: Stratigraphy and field relationships. *J Volcanol Geotherm Res* 136(3-4): 199–222.
- Sigurðsson H, et al. (2006) Marine investigations of Greece's Santorini volcanic field. *Eos* 87(34):337–348.
- Friedrich WL, et al. (2006) Santorini eruption radiocarbon dated to 1627–1600 B.C. *Science* 312(5773):548.
- Bacon CR (1983) Eruptive history of Mount Mazama and Crater Lake caldera, Cascade Range, USA. *J Volcanol Geotherm Res* 18(1-4):57–118.
- Zdanowicz CM, et al. (1999) Mount Mazama eruption: Calendrical age verified and atmospheric impact assessed. *Geology* 27(7):621–624.
- Dull R, et al. (2010) Did the TBJ Ilopango eruption cause the AD 536 event? American Geophysical Union, Fall Meeting 2010, December 13–17, 2010, San Francisco.
- Brown RJ, Vallance JW, Houghton BF, Hernandez W (2013) The AD 536 Phreatoplinian eruption of Volcán Ilopango, El Salvador: physical character of ash-rich pyroclastic-density-current deposits and coeval ash aggregates. IAVCEI 2013 Scientific Assembly, July 20–24, Kagoshima, Japan; poster, 3W-3G-P2.
- Pyle DM (2000) Sizes of volcanic eruptions. *Encyclopedia of Volcanoes*, eds Sigurðsson H, Houghton B, Rymer H, Stix J, McNutt S (Academic, San Diego), pp 263–269.
- Self S, Gertisser R, Thordarson T, Rampino MR, Wolff JA (2004) Magma volume, volatile emissions, and stratospheric aerosols from the 1815 eruption of Tambora. *Geophys Res Lett* 31: L20608.
- Wilson CJN, Walker GPL (1985) The Taupo eruption, New Zealand I. General aspects. *Philos Trans R Soc Lond A* 314(1529):199–228.
- Hogg A, Lowe DJ, Palmer J, Boswijk G, Bronk Ramsey C (2012) Revised calendar date for the Taupo eruption derived by 14C wiggle-matching using a New Zealand kauri 14C calibration data set. *Holocene* 22(4):439–449.
- Larsen JF (2006) Rhyodacite magma storage conditions prior to the 3430 yBP caldera-forming eruption of Aniakchak volcano, Alaska. *Contrib Mineral Petrol* 152(4):523–540.
- Begét J, Mason O, Anderson P (1992) Age, extent and climatic significance of the c. 3400 BP Aniakchak Tephra, Western Alaska, USA. *Holocene* 2(1):51–56.
- Pearce NJG, Westgate JA, Preece SJ, Eastwood WJ, Perkins WT (2004) Identification of Aniakchak (Alaska) tephra in Greenland ice core challenges the 1645 BC date for Minoan eruption of Santorini. *Geochem Geophys Geosyst* 5 (3):Q03005.
- Horn S, Schmincke HU (2000) Volatile emission during the eruption of Baitoushan volcano (China/North Korea) ca. 969 AD. *Bull Volcanol* 61(8):537–555.
- Xu J, et al. (2013) Climatic impact of the Millennium eruption of Changbaishan volcano in China: New insights from high-precision radiocarbon wiggle-match dating. *Geophys Res Lett* 40(1):54–59.
- Mothes PA, Hall ML (2008) The plinian fallout associated with Quilotoa's 800 yr BP eruption, Ecuadorian Andes. *J Volcanol Geotherm Res* 176(1):56–69.

18. Ledru MP, et al. (2013) The Medieval Climate Anomaly and the Little Ice Age in the eastern Ecuadorian Andes. *Climate of the Past* 9(1):307–321.
19. Fierstein J, Hildreth W (1992) The plinian eruptions of 1912 at Novarupta, Katmai National Park, Alaska. *Bull Volcanol* 54(8):646–684.
20. Self S, Rampino MR (1981) The 1883 eruption of Krakatau. *Nature* 294:699–704.
21. Williams SN, Self S (1983) The October 1902 plinian eruption of Santa Maria Volcano, Guatemala. *J Volcanol Geotherm Res* 16(1-2):33–56.
22. Hildreth W, Drake RE (1992) Volcan Quizapu, Chilean Andes. *Bull Volcanol* 54(2):93–125.
23. Carey S, Sigurdsson H (1987) Temporal variations in column height and magma discharge rate during the 79 A.D. eruption of Vesuvius. *Geol Soc Am Bull* 99:303–314.
24. Fontijn K, et al. (2011) The ~4-ka Rungwe Pumice (South-Western Tanzania): A wind-still Plinian eruption. *Bull Volcanol* 73(9):1353–1368.
25. Adams NK, et al. (2001) The physical volcanology of the 1600 eruption of Huaynaputina, southern Peru. *Bull Volcanol* 62(8):493–518.
26. Macías JL (2003) The 26 May 1982 breakout flows derived from failure of a volcanic dam at El Chichón, Chiapas, Mexico. *Geol Soc Am Bull* 116(1-2):233–246.

**Table S2. Geochemical composition of matrix glass from the Samalas pyroclastic fall deposits (electron microprobe analysis)**

| Oxide/element                         | F1 matrix glass |                  | F2 matrix glass |                  | F3 matrix glass |                  |
|---------------------------------------|-----------------|------------------|-----------------|------------------|-----------------|------------------|
|                                       | Mean            | ±1 $\sigma_{SD}$ | Mean            | ±1 $\sigma_{SD}$ | Mean            | ±1 $\sigma_{SD}$ |
| SiO <sub>2</sub> (wt.%)               | 66.66           | 1.6              | 67.11           | 1.35             | 67.47           | 1.39             |
| TiO <sub>2</sub> (wt.%)               | 0.47            | 0.11             | 0.45            | 0.1              | 0.43            | 0.1              |
| Al <sub>2</sub> O <sub>3</sub> (wt.%) | 16.04           | 0.37             | 15.87           | 0.28             | 15.5            | 0.49             |
| FeO (wt.%)                            | 2.77            | 0.19             | 2.57            | 0.21             | 2.56            | 0.2              |
| MnO (wt.%)                            | 0.14            | 0.06             | 0.14            | 0.07             | 0.14            | 0.06             |
| MgO (wt.%)                            | 0.74            | 0.07             | 0.67            | 0.05             | 0.61            | 0.09             |
| CaO (wt.%)                            | 2.22            | 0.16             | 2.08            | 0.14             | 1.78            | 0.19             |
| Na <sub>2</sub> O (wt.%)              | 3.99            | 0.33             | 3.84            | 0.37             | 3.74            | 0.3              |
| K <sub>2</sub> O (wt.%)               | 4.04            | 0.15             | 4.14            | 0.2              | 4.38            | 0.19             |
| P <sub>2</sub> O <sub>5</sub> (wt.%)  | 0.29            | 0.06             | 0.3             | 0.01             | 0.26            | 0.08             |
| S (ppm)                               | 94              | 63               | 58              | 29               | 57              | 45               |
| Cl (ppm)                              | 1,881           | 477              | 2,241           | 114              | 2,040           | 787              |
| F (ppm)                               | 359             | 110              | 307             | 85               | 272             | 134              |
| Total (wt.%)                          | 97.57           |                  | 97.43           |                  | 97.09           |                  |
| Na <sub>2</sub> O/K <sub>2</sub> O    | 0.99            |                  | 0.93            |                  | 0.85            |                  |
| N major                               | 85              |                  | 28              |                  | 52              |                  |
| N volatile                            | 72              |                  | 17              |                  | 61              |                  |
| Normalized to 100% for eight oxides   |                 |                  |                 |                  |                 |                  |
| SiO <sub>2</sub> (wt.%)               | 68.78           | 0.49             | 69.37           | 0.39             | 69.95           | 0.54             |
| TiO <sub>2</sub> (wt.%)               | 0.48            | 0.11             | 0.46            | 0.1              | 0.44            | 0.1              |
| Al <sub>2</sub> O <sub>3</sub> (wt.%) | 16.55           | 0.26             | 16.41           | 0.29             | 16.07           | 0.38             |
| FeO (wt.%)                            | 2.86            | 0.18             | 2.66            | 0.2              | 2.65            | 0.2              |
| MgO (wt.%)                            | 0.76            | 0.07             | 0.7             | 0.05             | 0.63            | 0.09             |
| CaO (wt.%)                            | 2.3             | 0.18             | 2.15            | 0.13             | 1.84            | 0.19             |
| Na <sub>2</sub> O (wt.%)              | 4.11            | 0.31             | 3.97            | 0.35             | 3.87            | 0.28             |
| K <sub>2</sub> O (wt.%)               | 4.17            | 0.15             | 4.28            | 0.18             | 4.54            | 0.18             |

Compositions was normalized to 100% for eight oxides to compare them with the available composition of the glass shard from the A.D. 1257–1259 event evidenced in the polar ice cores (1). *n* = number of analysis.

1. Sigurdsson H, Carey S (1989) Plinian and co-ignimbrite tephra fall from the 1815 eruption of Tambora volcano. *Bull Volcanol* 51(4):243–270.